

**BIOREGENERATION OF MONO-AMINE MODIFIED
SILICA AND GRANULAR ACTIVATED CARBON
LOADED WITH MONO-AZO DYES
IN BATCH SYSTEMS**

WAHEEBA AHMED ABDU AL-AMRANI

UNIVERSITI SAINS MALAYSIA

2013

**BIOREGENERATION OF MONO-AMINE MODIFIED
SILICA AND GRANULAR ACTIVATED CARBON
LOADED WITH MONO-AZO DYES
IN BATCH SYSTEMS**

by

WAHEEBA AHMED ABDU AL-AMRANI

Thesis submitted in fulfillment of the requirements for
the degree of
Doctor of Philosophy

December 2013

ACKNOWLEDGEMENTS

First of all, a great deal of gratitude is owed to my respected parents and their eternal support given with wishes and blessings are affectionately appreciated. Also, my exceptional thanks are extended to my sisters and brothers who always stood by me.

My infinite gratefulness and appreciation to my main supervisor Professor Lim Poh-Eng for his kind guidance, valuable suggestions, support, inspiration and encouragement extended during my study. I would also like to acknowledge my co-supervisors, Professor Madya Dr. Seng Chye-Eng and Professor Wan Saime Wan Ngah for their support throughout this research.

My very sincere gratitude goes to Mr. Abdul Razak, a staff member in the School of Chemical Sciences and Mr. Abdul Wahab, a chemical and equipment supplier who helped me in various instances during my study in Universiti Sains Malaysia (USM).

I am obliged to all my colleges, specially, Poh Ying, Kwok Yii, Wen Da, Kui Chew, Heng Chong, Siew Leng, Zhaung Gia, Sook Ling, Sui Yien, Run Hung, Muna Mastura, Nurul Farahana, Sangeetha and Affaizza who helped me in numerous ways and created friendly environment during my stay in Malaysia.

Last but not the least, the financial support from Ibb University-Yemen Scholarship is gratefully acknowledged.

TABLE OF CONTENTS

Acknowledgment	ii
Table of Contents	iii
List of Tables	ix
List of Figures	xii
List of Plates	xxii
List of Abbreviations	xxiii
List of Nomenclatures	xxiv
Abstrak	xxv
Abstract	xxviii

CHAPTER 1- INTRODUCTION

1.1	Background	1
1.2	History of Dyes	2
1.3	Classification of Dyes	3
	1.3.1 Azo Dye	4
1.4	Environmental Concerns	7
1.5	Dye Removal Techniques	8
	1.5.1 Adsorption	10
	1.5.1.1 Activated Carbon as Adsorbent	11
	1.5.1.2 Modified Silica Gel as Adsorbent	14
	1.5.2 Biodegradation of Azo Dyes	17
1.6	Regeneration of Spent Adsorbent	22
	1.6.1 Physical Regeneration	23
	1.6.2 Chemical Regeneration	27
	1.6.3 Biological Regeneration (Bioregeneration)	29
	1.6.3.1 Simultaneous Adsorption and Biodegradation Process	31
	1.6.3.2 Sequential Adsorption and Biodegradation Process	32

1.7	Mechanism of Bioregeneration Process	34
1.7.1	Exo-Enzymatic Reaction	35
1.7.2	Concentration Gradient	36
1.8	Factors Affecting Bioregeneration Process	38
1.8.1	Biodegradability of the Adsorbate	39
1.8.2	Reversibility of Adsorption	41
1.8.3	Porosity and Particle Size of Adsorbent	44
1.9	Quantification of the Bioregeneration Process	45
1.10	Bioregeneration of Spent Activated Carbon and Other Adsorbents	48
1.11	Objectives	49
CHAPTER 2- MATERIALS AND METHODS		51
2.1	Sequencing Batch Reactor	51
2.1.1	Experimental Set Up	51
2.1.2	Operation Mode	51
2.1.3	Preparation of Feed Solutions	54
2.1.3.1	Base Mix	54
2.1.3.2	Synthetic Azo Dye Wastewater	55
2.1.4	Culturing of Activated Biomasses	56
2.1.5	Evaluation of the Performance of SBRs	56
2.1.5.1	Mixed Liquid Suspended Solids Concentration	56
2.1.5.2	Settled Sludge Volume	57
2.1.5.3	Sludge Volume Index	57
2.1.5.4	Chemical Oxygen Demand Concentration	58
2.1.5.5	Bio-Decolorization of Azo Dyes	58
2.1.5.6	Bio-Mineralization of Azo Dye Intermediates	59
2.2	Characteristic of the Investigated Azo Dyes	59
2.2.1	Molecular Size of the Azo Dyes	60
2.2.2	Wavelength of Maximum absorbance for Azo Dyes	60

2.2.3	Stability of Azo Dyes	63
2.2.4	Solubility of Azo Dyes	64
2.3	Adsorption Studies	64
2.3.1	Preparation of Adsorbents	64
2.3.1.1	Granular Activated Carbon	64
2.3.1.2	Mono-Amine Modified Silica	64
2.3.1.3	Dried Biomass	65
2.3.2	Characterization of Adsorbents	65
2.3.2.1	Fourier Transform Infrared Spectroscopic Analyses	65
2.3.2.2	Surface Area and Pore Size Determinations	66
2.3.2.3	Scanning Electron Microscopic Analyses	67
2.3.2.4	Point of Zero Charge Determinations	67
2.3.3	Optimization of Parameters for Adsorption Study	68
2.3.3.1	Effect of Initial pH	68
2.3.3.2	Effect of Contact Time	69
2.3.3.3	Effect of Initial Azo Dye Concentration	69
2.3.4	Adsorption on Dried Biomass	70
2.3.5	Desorption of Azo Dye-Loaded Adsorbent	70
2.4	Regeneration Studies	72
2.4.1	Quantification of Regeneration Efficiency of the Spent Adsorbent	72
2.4.2	Effects of Operational Factors on Regeneration of Azo Dye-Loaded MAMS	75
2.4.2.1	Absence/Presence of Co-Substrate	75
2.4.2.2	Non-Acclimated Biomass	78
2.4.2.3	Initial AO7 Loading Concentration	79
2.4.2.4	Redox Conditions	80
2.4.2.5	Types of Acclimated Biomass	81
2.4.2.6	Initial AO7-Acclimated Biomass Concentration	82
2.4.2.7	Shaking Speed	83

2.4.2.8	Biomass Acclimation Concentration	83
2.4.2.9	Particle Size	84
2.4.3	Effects of Operational Factors on Regeneration of Azo Dye-Loaded GAC	85
2.4.3.1	Absence/Presence of Co-Substrate	85
2.4.3.2	Non-Acclimated Biomass	87
2.4.3.3	Initial AO7 Loading Concentration	88
2.4.4	Reusability of Bioregenerated MAMS Particles	89
2.4.5	Characterization of Acclimated Biomass	91
2.4.5.1	Scanning Electron Microscopy Analyses	91
CHAPTER 3- RESULTS AND DISCUSSION		92
3.1	Adsorbents	92
3.1.1	Synthesis of MAMS Particles	92
3.1.2	Characterization of Adsorbents	92
3.1.2.1	Fourier Transform Infrared Spectroscopic Analyses	94
3.1.2.2	Surface Area and Pore Size Determinations	96
3.1.2.3	Scanning Electron Microscopic Analyses	99
3.1.2.4	Point of Zero Charge Determinations	103
3.2	Adsorbates	104
3.2.1	UV-Vis Spectra of the Investigated Azo Dyes	104
3.2.2	Stability of the Azo Dyes	107
3.2.3	Solubility of the Azo Dyes	108
3.3	Adsorption Studies	108
3.3.1	Adsorption of Azo Dye on GAC and MAMS	108
3.3.1.1	Effect of Initial pH	108
3.3.1.2	Effect of Contact Time	112
3.3.1.3	Effect of Initial Azo Dye Concentration	115
3.3.1.4	Langmuir and Freundlich Isotherms	120

3.3.2	Adsorption of Azo Dye on Dried Biomass	128
3.3.3	Comparison of the Adsorption Capacities of the Adsorbents for Azo Dyes	131
3.4	Desorption of Azo Dye from Azo Dye-Loaded Adsorbents	131
3.5	Regeneration Studies	138
3.5.1	Effects of Operational Factors on Regeneration of Azo Dye-Loaded Adsorbents	138
3.5.1.1	Absence/Presence of the Co-Substrate	138
3.5.1.2	Using Non-Acclimated Biomass	165
3.5.1.3	Initial AO7 Loading Concentration	172
3.5.2	Comparison of Bioregeneration Efficiencies of the Azo Dye-Loaded Adsorbents	193
3.5.3	Effects of Operational Factors on Regeneration of AO7-Loaded MAMS	194
3.5.3.1	Redox Conditions	194
3.5.3.2	Types of Acclimated Biomass	200
3.5.3.3	Initial AO7-Acclimated Biomass Concentration	209
3.5.3.4	Shaking Speed	214
3.5.3.5	Biomass Acclimation Concentration	229
3.5.3.6	Particle Size	232
3.5.4	Reusability of Bioregenerated MAMS Adsorbent	259
3.6	Characterization of Azo Dye-Acclimated Biomass	270
CHAPTER 4- SUMMARY AND CONCLUSIONS		276
4.1	Desorption Studies	277
4.2	Bioregeneration Studies	278
4.3	Quantification of Bioregeneration	281
4.4	Recommendations for Future Research	282

REFERENCES	284
APPENDICES	303
LIST OF PUBLICATIONS AND PRESENTATION	326

LIST OF TABLES

		Page
Table 2.1	The operation periods of SBRs	53
Table 2.2	Base mix composition	55
Table 2.3	Physical and chemical properties of the investigated azo dyes	59
Table 2.4	Volume of the co-substrate used in the bioregeneration of azo dye-loaded MAMS under different protocols	77
Table 2.5	Operational modes for the regeneration of AO7-loaded MAMS particles	81
Table 3.1	The physical characteristics of the investigated adsorbents	98
Table 3.2	Parameters of non-linear Langmuir isotherm model, separation factor and correlation coefficient for the adsorption of azo dye on GAC and MAMS adsorbents at pH 2, the shaking speed of 200 rpm and 26 ± 1 °C	124
Table 3.3	Parameters of non-linear Freundlich isotherm and correlation coefficient for the adsorption of azo dye on GAC and MAMS adsorbents at pH 2, the shaking speed of 200 rpm and 26 ± 1 °C	125
Table 3.4	Parameters of non-linear Langmuir, Freundlich isotherm models and the correlation coefficient for the adsorption of azo dye on dried biomass at pH 6.6, the shaking speed of 200 rpm and 26 ± 1 °C	130
Table 3.5	Desorption percentage of the investigated azo dyes from the azo dye-loaded GAC and MAMS of particle size 0.25-0.42 mm at the shaking speed of 120 rpm and 26 ± 1 °C	134
Table 3.6	Regeneration efficiencies of the azo dye-loaded adsorbent particles using 300 mg/L of azo dye-acclimated biomass in the absence of co-substrate at the shaking speed of 120 rpm and 26 ± 1 °C	144

Table 3.7	Effect of the co-substrate volume on the bioregeneration efficiency of the AY9- and AR14-loaded adsorbents of particle size of 0.2-0.5 mm using azo dye-acclimated biomass at the shaking speed of 120 rpm and 26 ± 1 °C	162
Table 3.8	Bioregeneration efficiencies of azo dye-loaded adsorbents using 300 mg/L of the non-acclimated biomass in the absence and presence of the co-substrate at the shaking speed of 120 rpm and 26 ± 1 °C	171
Table 3.9	Regeneration efficiencies of AO7-loaded adsorbents at different initial AO7 loading concentrations under abiotic conditions at the shaking speed of 150 rpm and 26 ± 1 °C	180
Table 3.10	Regeneration efficiencies of AO7-loaded adsorbents at different initial AO7 loading concentrations under biotic conditions at the shaking speed of 150 rpm and 26 ± 1 °C	190
Table 3.11	Regeneration and COD removal efficiencies under different operational modes at the shaking speed of 150 rpm, initial biomass concentration of 300 mg/L and 26 ± 1 °C	198
Table 3.12	Regeneration efficiencies of AO7-loaded MAMS using 300 mg/L of different acclimated biomasses at the shaking speed of 150 rpm and 26 ± 1 °C under Modes I and II	208
Table 3.13	The COD removal efficiencies during the bioregeneration of AO7-loaded MAMS using 300 mg/L of different acclimated biomasses at the shaking speed of 150 rpm and 26 ± 1 °C under Modes I and II	209
Table 3.14	Bioregeneration efficiencies of AO7-loaded MAMS particles and total COD removal efficiencies under Mode II using different initial AO7-acclimated biomass concentrations at the shaking speed of 150 rpm and 26 ± 1 °C	212
Table 3.15	Regeneration efficiencies of AO7-loaded MAMS particles and total COD removal at different shaking speeds, 26 ± 1 °C and 300 mg/L of AO7-acclimated biomass concentration under different modes of operation	227

Table 3.16	Bioregeneration efficiencies of AO7-loaded MAMS adsorbent using 300 mg/L of biomass acclimated to different AO7 concentrations at the shaking speed of 150 rpm and 26 ± 1 °C	231
Table 3.17	Bioregeneration duration for the bioregeneration of AO7-, AY9-, and AR14-loaded MAM of different particle sizes using 300 mg/L of the respective azo dye-acclimated biomass at the shaking speed of 120 rpm and 26 ± 1 °C	245
Table 3.18	Regeneration efficiencies of AO7-loaded MAMS adsorbent of different particle sizes in the absence of co-substrate at the shaking speed of 120 rpm and 26 ± 1 °C under Modes I-IV	253
Table 3.19	Regeneration efficiencies of AY9- and AR14-loaded MAMS adsorbents of different particle size ranges in the presence of co-substrate at the shaking speed of 120 rpm and 26 ± 1 °C under Mode II	254
Table 3.20	Bioregeneration efficiencies and capacity losses of AO7-loaded MAMS without and with microbial fouling removal at the shaking speed of 150 rpm and 26 ± 1 °C under Mode II	262
Table 3.21	The COD concentrations, mg/L, of the washings of the bioregenerated AO7-loaded MAMS with distilled water and de-fouling reagent solution in three successive cycles of use	264

LIST OF FIGURES

		Page
Figure 1.1	Chemical structures of different types of azo dyes	5
Figure 1.2	Proposed mechanism for reduction of azo dye by whole bacterial cells	18
Figure 1.3	General overview of the fate of azo dyes and aromatic amines during anaerobic-aerobic treatment	19
Figure 2.1	Schematic diagram of sequencing batch reactor (SBR) for culturing the azo dyes-acclimated biomasses	52
Figure 2.2	The chemical structures of the investigated azo dyes	61
Figure 2.3	The molecular sizes of (a) AO7, (b) AY9 and (c) AR14 using Chem Office 3D Ultra 12.	62
Figure 3.1	Modification of silica surface using 3-Aminopropylethoxy-silane (3-APTS)	93
Figure 3.2	FTIR spectra of (a) GAC, (b) unmodified silica gel and (c) MAMS adsorbents	95
Figure 3.3	Determination of the points of zero charge of the investigated adsorbents	103
Figure 3.4	UV-Vis spectra of (a) AO7, (b) AY9, and (c) AR14	105
Figure 3.5	Tautomers of (a) AO7 and (b) AR14 in their aqueous phase	106
Figure 3.6	Amounts of AO7, AY9 and AR14 adsorbed on (a) GAC (0.25-0.42 mm), (b) MAMS (0.84-2.00 mm), (c) MAMS (0.25-0.42 mm) and (d) MAMS (0.063-0.100 mm) at different pHs	109
Figure 3.7	Effect of contact time on the adsorption of AO7, AY9 and AR14 on (a) GAC (0.25-0.42 mm), (b) MAMS (0.84-2.00 mm), (c) MAMS (0.25-0.42 mm) and (d) MAMS (0.063-0.100 mm).	113

Figure 3.8	Effect of the initial azo dye concentration of AO7, AY9 and AR14 on (a) GAC (0.25-0.42 mm), (b) MAMS (0.84-2.00 mm), (c) MAMS (0.25-0.42 mm) and (d) MAMS (0.063-0.100 mm)	116
Figure 3.9	Experimental (solid bullets) and calculated (dash line) isotherms for the adsorption of AO7, AY9 and AR14 on (a) GAC (0.25-0.42 mm), (b) MAMS (0.84-2.00 mm), (c) MAMS (0.25-0.42 mm) and (d) MAMS (0.063-0.100 mm)	122
Figure 3.10	Adsorption isotherm of the investigated azo dye on the dried biomass in the presence of nutrients at the shaking speed of 200 rpm, pH 6.62 and 26 ± 1 °C	129
Figure 3.11	Time courses of the concentration of the investigated azo dye desorbed in (a) distilled water, (b) nutrients and (c) NaOH (pH 9) solutions due to the desorption from azo dye-loaded GAC at the shaking speed of 120 rpm	132
Figure 3.12	Time courses of the concentration of the investigated azo dye desorbed in (a) distilled water, (b) nutrients and (c) NaOH (pH 9) solutions due to the desorption from azo dye-loaded GAC at the shaking speed of 120 rpm	133
Figure 3.13	Time courses of (a) concentration of azo dye, (b) ORP, and (c) DO concentration in the bulk solution during the regeneration of azo dye-loaded GAC in the absence of co-substrate at the shaking speed of 120 rpm.	139
Figure 3.14	Time courses of (a) concentration of azo dye, (b) ORP, and (c) DO concentration in the bulk solution during the regeneration of azo dye-loaded MAMS in the absence of co-substrate at the shaking speed of 120 rpm	140
Figure 3.15	Time courses of AY9 concentration in the bulk solution in the first stage during the bioregeneration of AY9-loaded MAMS using Protocols (a) A, (b) B and (c) C at the shaking speed of 120 rpm	146
Figure 3.16	Time courses of ORP during the first stage of the bioregeneration of AY9-loaded MAMS particles using Protocols (a) A, (b) B and (c) C at the shaking speed of 120 rpm	147

Figure 3.17	Time courses of DO concentration during the bioregeneration of AY9-loaded MAMS particles using Protocols of (a) A, (b) B and (c) C at the shaking speed of 120 rpm	148
Figure 3.18	Time courses of (a) AR14 concentration, (b) ORP, (c) DO concentration and (d) pH in the bulk solution during the bioregeneration of AR14-loaded MAMS with co-substrate using protocols B and C at the shaking speed of 120 rpm	151
Figure 3.19	Time courses of SA concentrations of during the bioregeneration of AY9-loaded MAMS particles using Protocols (a) B (25.8 mL of the co-substrate) and (b) C (different volumes of the co-substrate)	154
Figure 3.20	Time courses of the (a) concentrations of AY9 and AR14, (b) ORP, (c) DO concentration and (d) pH during the bioregeneration of AY9-and AR14-loaded GAC under Protocol B using 25.8 mL of co-substrate	157
Figure 3.21	Time courses of the (a) concentrations of AY9 and AR14, (b) ORP and (c) DO concentration during the bioregeneration of AY9-and AR14-loaded GAC under Protocol B using 40 mL of co-substrate	159
Figure 3.22	Time courses of pH change during the bioregeneration of AY9-loaded MAMS under Protocols (a) A, (b) B and (c) C at the shaking speed of 120 rpm	164
Figure 3.23	Time courses of the desorbed azo dye concentration from azo dye-loaded (a) GAC and (b) MAMS during the regeneration process using non-acclimated biomass in the absence of co-substrate	166
Figure 3.24	Time courses of the desorbed azo dye concentration from azo dye-loaded (a) GAC and (b) MAMS during the regeneration process using non-acclimated biomass in the presence of the co-substrate	167
Figure 3.25	Time courses of ORP values during the bioregeneration of azo dye-loaded (a) GAC and (b) MAMS during the regeneration process using non-acclimated biomass in the	168

presence of the co-substrate

Figure 3.26	Time courses of ORP values during the regeneration of azo dye-loaded (a) GAC and (b) MAMS during the regeneration process using non-acclimated biomass in the absence of the co-substrate	169
Figure 3.27	Time courses of the AO7 concentration during the regeneration of AO7-loaded (a) GAC and (b) MAMS at different AO7 initial loading concentrations under abiotic conditions at the shaking speed of 150 rpm	173
Figure 3.28	Time courses of pH in the regeneration process of AO7-loaded (a) GAC and (b) MAMS at different AO7 initial loading concentrations under abiotic conditions at the shaking speed of 150 rpm	176
Figure 3.29	Time courses of ORP during the regeneration process of AO7-loaded (a) GAC and (b) MAMS at different AO7 initial loading concentrations under abiotic conditions	177
Figure 3.30	Time courses of the COD concentration during the regeneration process of AO7-loaded MAMS at different initial loading of AO7 at the shaking speed of 150 rpm	179
Figure 3.31	Time courses of the AO7 concentration in the first stage during the regeneration of AO7-loaded (a) GAC and (b) MAMS at different AO7 initial loading concentrations under biotic conditions at the shaking speed of 150 rpm and 26 ± 1 °C	182
Figure 3.32	Time courses of ORP in the first stage during the regeneration of AO7-loaded (a) GAC and (b) MAMS at different AO7 initial loading concentrations under biotic conditions at the shaking speed of 150 rpm and 26 ± 1 °C	183
Figure 3.33	UV-Visible spectra of (a) AO7 as a function of time in the first stage (without aeration) and (b) SA as a function of time at the second stage (full aeration) during the regeneration of AO7-loaded MAMS at initial loading of 400 mg/L	185

Figure 3.34	Time courses of the SA concentration in the second stage (full aeration) during the bioregeneration of AO7-loaded (a) GAC and (b) MAMS at different AO7 initial loading concentrations.	187
Figure 3.35	Time courses of COD concentration during the bioregeneration of AO7-loaded MAMS at the different initial AO7 loading concentrations at the shaking speed of 150 rpm and 26 ± 1 °C	188
Figure 3.36	Time courses of pH values during the regeneration of AO7-loaded (a) GAC and (b) MAMS at different initial AO7 loading concentrations under biotic conditions, shaking speed of 150 rpm and 26 ± 1 °C	192
Figure 3.37	Time courses of the concentrations of (a) AO7 in the first stage, (b) SA in the second stage and (c) COD during the bioregeneration of AO7-loaded MAMS using 300 mg/L of initial biomass concentration at the shaking speed of 150 rpm and 26 ± 1 °C under different operational modes	195
Figure 3.38	Time courses of (a) pH, (b) DO concentration and (c) ORP in the bulk solution during the bioregeneration of AO7-loaded MAMS using 300 mg/L of initial biomass concentration at the shaking speed of 150 rpm and 26 ± 1 °C under different operational modes	196
Figure 3.39	Time courses of (a) AO7 concentration, (b) Optical density and (c) COD concentration in the bulk solution during the bioregeneration of AO7-loaded MAMS at the shaking speed of 150 rpm and 26 ± 1 °C using 300 mg/L of different types of acclimated biomass under Mode I	202
Figure 3.40	Time courses of (a) DO concentration and (b) pH in the bulk solution during the bioregeneration of AO7-loaded MAMS at the shaking speed of 150 rpm and 26 ± 1 °C using 300 mg/L of different types of acclimated biomass under Mode I	203
Figure 3.41	Time courses of (a) concentrations of AO7, (b) optical density and (c) COD concentration in the bulk solution during the bioregeneration of AO7-loaded MAMS using different acclimated biomasses under Mode II	204

Figure 3.42	Time courses of (a) ORP, (b) DO concentration and (c) pH in the bulk solution during the bioregeneration of AO7-loaded MAMS at the shaking speed of 150 rpm and 26 ± 1 °C using 300 mg/L of different types of acclimated biomass under Mode II	205
Figure 3.43	Time courses of the concentrations of (a) AO7 in the first stage, (b) SA in the second stage and (c) COD during the bioregeneration of AO7-loaded MAMS using different initial AO7-acclimated biomass concentrations at the shaking speed of 150 rpm and 26 ± 1 °C under Mode II	211
Figure 3.44	Time courses of (a) ORP in the first stage, (b) pH during the bioregeneration of AO7-loaded MAMS using different initial AO7-acclimated biomass concentrations at the shaking speed of 150 rpm and 26 ± 1 °C under Mode II	213
Figure 3.45	Time courses of AO7 concentration in the first stage under Modes (a) I and (b) II during the regeneration of AO7-loaded MAMS particles (0.25-0.42 mm) at different shaking speeds under abiotic conditions at 26 ± 1 °C	215
Figure 3.46	Time courses of pH in the first stage under Modes (a) I, and (b) II during the regeneration of AO7-loaded MAMS particles (0.25-0.42 mm) at different shaking speeds under abiotic conditions at 26 ± 1 °C	216
Figure 3.47	Time courses of AO7 concentration in the first stage under Modes (a) I and (b) II during the regeneration of AO7-loaded MAMS particles (0.25-0.42 mm) at different shaking speeds under biotic conditions at 26 ± 1 °C	218
Figure 3.48	Time courses of the optical density under Modes (a) I, (b) II and (c) III during the regeneration of AO7-loaded MAMS particles (0.25-0.42 mm) at different shaking speeds using biotic conditions at 26 ± 1 °C	219
Figure 3.49	Time courses of SA concentration in the second stage under Modes (a) I, (b) II and (c) III during the regeneration of AO7-loaded MAMS particles (0.25-0.42 mm) at different shaking speeds under biotic conditions at 26 ± 1 °C	220

Figure 3.50	Time courses of DO concentration under Modes (a) I, (b) II and (c) III during the regeneration of AO7-loaded MAMS particles (0.25-0.42 mm) at different shaking speeds under biotic conditions at 26 ± 1 °C	221
Figure 3.51	Time courses of ORP under Modes (a) II and (b) III during the regeneration of AO7-loaded MAMS particles (0.25-0.42 mm) at different shaking speeds under biotic conditions at 26 ± 1 °C	222
Figure 3.52	Time courses of COD concentration under Modes (a) I, (b) II and (c) III during the regeneration of AO7-loaded MAMS particles (0.25-0.42 mm) at different shaking speeds under biotic conditions at 26 ± 1 °C	223
Figure 3.53	Time courses of pH under Modes (a) I, (b) II and (c) III during the bioregeneration of AO7-loaded MAMS particles (0.25-0.42 mm) at different shaking speeds under biotic conditions at 26 ± 1 °C	228
Figure 3.54	Time courses of (a) AO7 concentration in the first stage and (b) SA concentration in the second stage during the bioregeneration of AO7-loaded MAMS using biomasses at different AO7 concentration acclimation under Mode II and the shaking speed of 120 rpm	230
Figure 3.55	Time courses of (a) AO7 concentration, (b) pH and (c) DO concentration during the regeneration of AO7-loaded MAMS of different particle sizes under Mode I and abiotic condition and at shaking speed of 120 rpm and 26 ± 1 °C	233
Figure 3.56	Time courses of (a) AO7 concentration, (b) pH, (c) DO concentration and (d) ORP during the regeneration of AO7-loaded MAMS of different particle sizes under Mode II and abiotic condition and at the shaking speed of 120 rpm and 26 ± 1 °C	234
Figure 3.57	Time courses of (a) AY9 concentration, (b) pH, (c) DO concentration and (d) ORP during the regeneration of AY9-loaded MAMS at different particle sizes under Mode II and abiotic condition and at the shaking speed of 120 rpm and 26 ± 1 °C	236

Figure 3.58	Time courses of (a) AR14 concentration, (b) pH, (c) DO concentration and (d) ORP during the regeneration of AR14-loaded MAMS at different particle sizes under Mode II and abiotic condition at the shaking speed of 120 rpm and 26 ± 1 °C	238
Figure 3.59	Time courses of AO7 concentrations during the bioregeneration of AO7-loaded MAMS of different particle sizes in the first stage under Modes (a) I, (b) II and (c) III at shaking speed of 120 rpm and 26 ± 1 °C	242
Figure 3.60	Time courses of AY9 concentration during the bioregeneration of AY9-loaded MAMS of different particle sizes in the first stage under Mode II in the presence of co-substrate using protocols (a) B and (b) C at the shaking speed of 120 rpm and 26 ± 1 °C	243
Figure 3.61	Time courses of AR14 concentration during the bioregeneration of AR14-loaded MAMS of different particle sizes in the first stage under Mode II in the presence of co-substrate using protocols (a) B and (b) C at the shaking speed of 120 rpm and 26 ± 1 °C	244
Figure 3.62	Time courses of SA concentration in the second stage during the bioregeneration of AO7-loaded MAMS of different particle sizes under Modes (a) I, (b) II and (c) III at the shaking speed of 120 rpm and 26 ± 1 °C	247
Figure 3.63	Time courses of SA concentration in the second stage during the bioregeneration of AY9-loaded MAMS of different particle sizes using protocols (a) B and (b) C at the shaking speed of 120 rpm and 26 ± 1 °C	248
Figure 3.64	Time courses of DO concentration during the bioregeneration of AR14-loaded MAMS at the different particle sizes using protocols (a) B and (b) C at the shaking speed of 120 rpm and 26 ± 1 °C	249
Figure 3.65	Time courses of DO concentration during the bioregeneration of AO7-loaded MAMS of different particle sizes under Modes (a) I, (b) II and (c) III at the shaking speed of 120 rpm and 26 ± 1 °C	250

Figure 3.66	Time courses of DO concentration during the bioregeneration of AY9-loaded MAMS of different particle sizes using protocols (a) B and (b) C at the shaking speed of 120 rpm and 26 ± 1 °C	251
Figure 3.67	Time courses of pH during the bioregeneration of AO7-loaded MAMS of different particle sizes under Modes (a) I, (b) II and (c) III at shaking speed of 120 rpm and 26 ± 1 °C	256
Figure 3.68	Time courses of pH during the bioregeneration of AY9-loaded MAMS of different particle sizes using protocols (a) B and (b) C at the shaking speed of 120 rpm and 26 ± 1 °C	257
Figure 3.69	Time courses of pH concentrations during the bioregeneration of AR14-loaded MAMS at the different particle sizes using Protocols (a) B and (b) C at the shaking speed of 120 rpm and 26 ± 1 °C	258
Figure 3.70	Time courses of AO7 concentration in the bulk solution in the first stage of the bioregeneration of AO7-loaded MAMS for three cycles of use under (a) without microbial de-fouling and (b) with microbial de-fouling removal treatment at the shaking speed of 150 rpm and 26 ± 1 °C	261
Figure 3.71	Time courses of SA concentration in the bulk solution in the second stage during the bioregeneration of AO7-loaded MAMS in three cycles of use under Mode II (a) without microbial de-fouling and (b) with microbial de-fouling treatment at the shaking speed of 150 rpm and 26 ± 1 °C	265
Figure 3.72	Time courses of COD concentration in the bulk solution during the bioregeneration of AO7-loaded MAMS in three cycles of use under Mode II (a) without microbial de-fouling and (b) with microbial de-fouling treatment at the shaking speed of 150 rpm and 26 ± 1 °C	267
Figure 3.73	Time courses of pH in the bulk solution during the bioregeneration of AO7-loaded MAMS in three cycles of use (a) without microbial de-fouling and (b) with microbial de-fouling treatment at the shaking speed of 150 rpm and 26 ± 1 °C	268

Figure 3.74 Time courses of ORP in bulk solution during the first stage of bioregeneration of AO7-loaded MAMS in three cycles of use (a) without microbial de-fouling and (b) with microbial de-fouling treatment at the shaking speed of 150 rpm and 26 ± 1 °C 269

LIST OF PLATES

		Page
Plate 3.1	SEM images of GAC with magnifications of (a) 500 x and (b) 10 k x	100
Plate 3.2	SEM images of silica gel with magnifications of (a) 200 x and (b) 10 k x	101
Plate 3.3	SEM images of MAMS with magnification of (a) 170 x and (b) 10 k x	102
Plate 3.4	SEM images of (a) azo dye-free biomass, (b) AO7-acclimated biomass, (c) AY9-acclimated biomass and (d) AR14-acclimated biomass used in the bioregeneration of azo dye-loaded GAC and MAMS adsorbents	272
Plate 3.5	SEM images (magnification of 2 k x) of the AO7-acclimated biomass attached on (a) GAC and (b) MAMS surfaces after bioregeneration process under Mode II	274
Plate 3.6	SEM images (magnification of 5 k x) of the AO7-acclimated biomass attached on (a) GAC and (b) MAMS surfaces after bioregeneration process under Mode II	275

LIST OF ABBREVIATIONS

AO7	Acid Orange 7
AY9	Acid Yellow 9
AR14	Acid Red 14
MAMS	Mono-Amine Modified Silica
GAC	Granular Activated Carbon
PAC	Powdered Activated Carbon
C.I.	Color Index
COD	Chemical Oxygen Demand
AC	Activated Carbon
MS	Modified Silica
3-APTS	3-Aminopropyltriethoxysilane
SBR	Sequencing Batch Reactor
MLSS	Mixed Liquid Suspended Solids
SV ₃₀	Settled Sludge Volume
SVI	Sludge Volume Index
DB	Dried Biomass
FTIR	Fourier Transform Infrared Spectroscopy
SEM	Scanning Electron Microscopy
PZC	Point of Zero Charge
DO	Dissolved Oxygen
ORP	Oxygen Reduction Potential
UV-Vis	Ultraviolet-Visible
1A2N	1-Amino-2-Naphthol
SA	Sulfanilic Acid
OD _{610nm}	Optical Density at wavelength of 610 nm
SD	Standard Deviation

LIST OF NOMENCLATURE

C_t	Residual azo dye concentration, mg/L, in the bulk solution at different time intervals
C_i	Initial azo dye concentration, mg/L, at zero time
C_e	Equilibrium azo dye concentration, mg/L, in the bulk solution
Q_t	Amount of adsorbed azo dye per unit weight of adsorbent, mg/g, at t of the contact time
Q_e	Equilibrium amount of adsorbed azo dye per unit weight of adsorbent, mg/g
Q_{reload}	Amount of adsorbed azo dye per unit weight of regenerated adsorbent, mg/g
Q_{sat}	Amount of adsorbed azo dye per unit weight of adsorbent, mg/g, at the saturation case
Q_{il}	Initial amount adsorbed of azo dye o adsorbent, mg/g, in the first cycle during the adsorption-bioregeneration cycles
Q_{max}	Theoretical maximum amount adsorbed of azo dye per unit weight of adsorbent, mg/g, in Langmuir isotherm model
K_F	Freundlich parameter related to the adsorption capacity of the adsorbent, $(\text{mg/g}) (\text{L/mg})^{1/n}$
K_L	Binding constant of adsorbate-adsorbent, L/mg, in Langmuir isotherm model
R_L	A dimensionless constant called the separation factor
n	A dimensionless constant related to the strength of adsorbate-adsorbent in Freundlich isotherm model
C_{inf}	Azo dye concentration in the influent
C_{eff}	Azo dye concentration in the effluent

BIOREGENERASI SILIKA TERUBAHSUAI DENGAN MONO-AMINA DAN KARBON TERAKTIF BUTIRAN YANG DITAMBAH DENGAN PENCELUP MONO-AZO DALAM SISTEM KELOMPOK

ABSTRAK

Objektif kajian ini adalah untuk mengkaji dan membandingkan tempoh masa dan kecekapan bioregenerasi bagi silika terubahsuai mono-amina (MAMS) dan butiran karbon teraktif (GAC) termuat dengan pencelup azo, iaitu Asid Oren 7 (AO7), Asid Kuning 9 (AY9) dan Asid Merah 14 (AR14) dengan menggunakan pendekatan penjerapan dan biodegradasi secara berturutan dalam sistem kelompok. Kecekapan bioregenerasi GAC dan MAMS yang termuat dengan setiap satu pencelup azo dikuantifikasikan dengan menggunakan pengukuran langsung atas kandungan pencelup azo pada penjerap dengan memuatkan semula penjerap terbioregenerasi. Selain itu, faktor operasi yang mempengaruhi bioregenerasi MAMS yang termuat dengan pencelup azo, iaitu kehadiran/ketiadaan subtrak bersama, biojisim yang teraklimatisasi/tidak-teraklimatisasi, kepekatan muatan awal AO7, keadaan redoks, jenis biojisim yang teraklimatisasi, kepekatan awal biojisim AO7-teraklimatisasi, kelajuan penggoncangan, kepekatan aklimasi biojisim dan saiz partikel telah ditinjau secara terperinci.

Kecekapan bioregenerasi GAC yang termuat dengan AO7 dikaji berada dalam lingkungan 3-15% sahaja, manakala kecekapan bioregenerasi MAMS yang termuat dengan AO7 didapati berada dalam lingkungan 79-90% pada kepekatan muatan awal AO7 yang berlainan. Bagi bioregenerasi GAC yang termuat dengan AY9 dan AR14, kecekapan bioregenerasi didapati masing-masing berada dalam lingkungan 28-30% dan 20-21%, manakala kecekapan bioregenerasi MAMS yang termuat dengan AY9

and AR14 didapati mencapai hampir 100% bagi saiz partikel MAMS yang berlainan. Keputusan menunjukkan kecekapan bioregenerasi yang rendah bagi GAC yang termuat dengan pencelup azo berbanding dengan MAMS disebabkan oleh penyahjerapan yang lemah bagi pencelup azo dari permukaan GAC.

Bioregenerasi MAMS yang termuat dengan AO7 pada keadaan redoks yang berlainan menunjukkan bahawa aplikasi dua peringkat yang melibatkan penyahjerapan/bio- penyahwarnaan pencelup azo dalam larutan pukal dengan atau tanpa pengudaraan dalam peringkat pertama, diikuti dengan bio-mineralisasi yang sempurna bagi sebatian perantaraannya dalam peringkat kedua dengan pengudaraan penuh mempertingkatkan kecekapan bioregenerasi MAMS yang termuat dengan AO7 serta jumlah penyingkiran COD. Bioregenerasi partikel MAMS yang termuat dengan AO7 pada kelajuan penggoncangan yang berlainan, iaitu 100, 120, 150, dan 180 rpm menunjukkan bahawa peningkatan kelajuan penggoncangan akan meningkatkan tempoh masa bioregenerasi disebabkan oleh penurunan kepekatan biojisim dengan peningkatan kelajuan penggoncangan tetapi tidak memberi kesan yang nyata atas kecekapan bioregenerasi.

Kajian bioregenerasi MAMS yang termuat dengan AO7, AY9 dan AR14 dengan saiz partikel yang berlainan menunjukkan bahawa tempoh masa bioregenerasi meningkat dengan penyusutan saiz partikel MAMS. Tambahan pula, kecekapan bioregenerasi MAMS yang termuat dengan AO7 menurun dengan mendadak dengan penyusutan saiz partikel MAMS daripada 0.84-2.00 mm kepada 0.24-0.42 mm dan kepada 0.063-0.100 mm.

Kebolehgunaan semula MAMS yang termuat dengan AO7 terbioregenerasi bagi tiga kitaran tanpa dan dengan rawatan pembersihan mikrob menunjukkan kemerosotan keupayaan penjerapan oleh MAMS secara beransuran bagi kedua-dua kes dengan kemerosotan keupayaan penjerapan yang lebih tinggi bagi kes tanpa rawatan pembersihan mikrob berbanding (23-47%) dengan kes rawatan pembersihan mikrob (17-33%).

BIOREGENERATION OF MONO-AMINE MODIFIED SILICA AND GRANULAR ACTIVATED CARBON LOADED WITH MONO-AZO DYES IN BATCH SYSTEMS

ABSTRACT

The objectives of this study were to investigate and compare the durations and efficiencies of bioregeneration of granular activated carbon (GAC) and mono-amine modified silica (MAMS) loaded with mono-azo dyes, namely Acid Orange 7 (AO7), Acid Yellow 9 (AY9) and Acid Red 14 (AR14) using sequential adsorption and biodegradation approach in batch systems. The bioregeneration efficiencies of GAC and MAMS loaded with each azo dye were quantified using the direct measurement of the azo dye content on the adsorbent by reloading the bioregenerated adsorbent. Additionally, some operational factors affecting the bioregeneration of azo dye-loaded MAMS, namely the presence/absence of co-substrate, acclimated/non-acclimated biomass, initial AO7 loading concentration, redox condition, type of acclimated biomass, initial AO7-acclimated biomass concentration, shaking speed, biomass acclimation concentration, and particle size were extensively investigated.

The bioregeneration efficiencies of AO7-loaded GAC were found to be in the range of 3-15% only whereas the bioregeneration efficiencies of AO7-loaded MAMS were found to be in the range of 70-90% at different initial AO7 loading concentrations. As for the bioregeneration of AY9- and AR14-loaded GAC, the bioregeneration efficiencies were found to be in the range of 28-30% and 20-21%, respectively, whereas the bioregeneration efficiencies of AY9- and R14-loaded MAMS were found to be mostly 100% for different particle sizes of MAMS. The results demonstrated low

bioregeneration efficiencies of azo dye-loaded GAC compared to those on MAMS due to poor desorption of the azo dye from the GAC surface.

Bioregeneration of AO7-loaded MAMS at different redox conditions revealed that application of two stages involving the desorption/bio-decolorization of the azo dye in the bulk solution with or without aeration in the first stage followed by complete biomineralization of its intermediate compounds in the second stage under full aeration enhanced the bioregeneration efficiency of AO7-loaded MAMS and total COD removal. Bioregeneration of AO7-loaded MAMS particles at different shaking speeds, namely 100, 120, 150, and 180 rpm showed that increasing the shaking speed would increase the bioregeneration duration due to decreasing biomass concentration with increasing shaking speed but did not have an observable effect on the bioregeneration efficiency.

Studies of the bioregeneration of AO7-, AY9- and AR14-loaded MAMS of different particle sizes showed that the bioregeneration duration increased with decreasing particle size of MAMS. In addition, the bioregeneration efficiencies of AO7-loaded MAMS decreased drastically with decreasing particle size of MAMS from 0.84-2.00 mm to 0.24-0.42 mm and to 0.063-0.100 mm.

The reusability of bioregenerated AO7-loaded MAMS particles for three cycles of use without and with microbial de-fouling treatment demonstrated the progressive deterioration of the adsorption capacity of MAMS for both cases with a higher total capacity loss for the case without microbial de-fouling treatment (23-47%) compared to that with microbial de-fouling treatment (17-33%).

CHAPTER 1

INTRODUCTION

1.1 Background

The development of science and technologies has improved the quality of human life to a great extent. However, many environmental problems remain and need to be solved. Among these problems is the problem of fresh water shortage as a result of population growth. Textile industry is one of the most important and rapidly developing industrial sectors in the world after the scientists discovered the synthetic dyes. Dye factories across the world are discharging millions of tons of dye effluent into receiving water courses. Therefore, there is an urgent need for the installation of wastewater treatment systems to treat the dye-bearing wastewaters before they are discharged to the environment to prevent further contamination of the limited water resources.

One of the challenging issues for chemists is to pursue green(er), safe(er) and clean(er) dye removal technique due to the huge amount of toxic wastes and byproducts arising from using the chemical processes (Robinson et al., 2001; Gupta and Suhas, 2009). Unfortunately, cleaner dye wastewater treatment methods imply higher energy/operation costs. Nonetheless, significant reduction of costs and/or enhancement of dye removal can be achieved using a combination of different methods in hybrid treatments (Anjaneyulu et al., 2005). Combined an adsorption technique with a bioregeneration process of the spent adsorbent is one of the safer and greener methods in pollution control due to the environmentally friendly nature and cost-effectiveness of the process (Aktas and Çeçen, 2007; Ng et al., 2009). Consequently, this research is

primarily focused on the removal of azo dyes, specifically Acid Orange 7 (AO7), Acid Yellow 9 (AY9) and Acid Red 14 (AR14) using an adsorption technique followed by bioregeneration process for the azo dye-loaded adsorbents, namely granular activated carbon (GAC) and mono-amine modified silica (MAMS) under sequential adsorption and biodegradation approach using batch systems. The investigated azo dyes are water soluble anionic dyes used in the dyeing of natural fibers, modified acrylic, textile, silk, leather, wool and paper (Daneshvar and Khataee, 2006; Daneshvar et al., 2008), whereas AR14 is used in the food industry as well .

1.2 History of Dyes

Throughout the history of mankind, people have been using colorants for the painting and dyeing of their surroundings, their skins and their clothes. Until the middle of the 19th century, all colorants applied were from natural origin. These dyes are all aromatic compounds, originating usually from plants (e.g. the red dye alizarin from madder and indigo from wood), insects (e.g. the scarlet dye kermes from the shield-louse *Kermes vermilio*), fungi and lichens (Balter, 2009).

Synthetic dye manufacturing started in 1856, when the English chemist, William Henry Perkin, in an attempt to synthesize quinine, obtained instead a bluish substance with excellent dyeing properties that later became known as aniline purple, tyrian purple or mauveine. Perkin patented his invention and set up a production line (Rai et al., 2005; Saratale et al., 2011). In the beginning of the 20th century, synthetic dyes quickly replaced the traditional natural dyes due to lower cost. In addition, they offered a vast range of new colors, and imparted better properties to the dyed materials

(Zollinger, 2003). This has led to a higher consumption of synthetic dyes over natural dyes for most types of industrial applications. There are more than 8000 chemical products associated with the dyeing process listed in the color index, while over 100,000 commercially available dyes exist with over 7×10^5 metric tons of dyestuff produced annually (Zollinger, 1987).

1.3 Classification of Dyes

All aromatic compounds absorb electromagnetic energy but only those that absorb light with wavelengths in the visible range (~350-700 nm) are colored. Dyes contain chromophores, *i.e.* de-localized electron systems with conjugated double bonds, and auxo-chromes, *i.e.* electron-withdrawing or electron donating substituent that cause or intensify the color of the chromophore by altering the overall energy of the electron system. Usual chromophores are -C=C-, -C=N-, -C=O, -N=N-, -NO₂ and quinoid rings whereas usual auxo-chromes are -NH₂, -COOH, -SO₃H and -OH. Therefore, according to dye structure or chromophore, 20-30 different groups of dyes can be discerned. Azo (monoazo, diazo, triazo, polyazo), anthraquinone, phthalocyanine and triarylmethane dyes are quantitatively the most important groups. Other groups are diarylmethane, indigoid, azine, oxazine, thiazine, xanthene, nitro, nitroso, methine, thiazole, indamine, indophenol, lactone, aminoketone and hydroxyketone dyes and dyes of undetermined structure (stilbene and sulphur dyes) (Abrahart, 1968; Rai et al., 2005). There is only a single example for the presence of an azo group in a natural product (4,4'-dihydroxyazobenzene) (Stolz, 2001).

In addition, the vast array of commercial colorants is classified in terms of color, structure and application method in the Color Index (C.I.) which is edited since 1924 by the Society of Dyers and Colorists and the American Association of Textile Chemists and Colorists. Each different dye is given a C.I. generic name determined by its application characteristics and its color. The Color Index (3rd addition) discerns 15 different application classes, namely acid dyes, reactive dyes, metal complex dyes, direct dyes, basic dyes, mordant dyes, disperse dyes, pigment dyes, vat dyes, anionic dyes and ingrain dyes, sulfur dyes, solvent dyes, fluorescent brighteners, food dyes and natural dyes. Food dyes are not used as textile dyes and the use of natural dyes (mainly anthraquinone, indigoid, flavenol, flavone or chroman compounds that can be used as mordant, vat, direct, acid or solvent dyes) in textile-processing operations is very limited. Generally, the dyes used in the textile industry are basic dyes, acid dyes, reactive dyes, direct dyes, azo dyes, mordant dyes, vat dyes, disperse dyes and sulfur dyes. Azo derivatives are the major class of dyes that are used in the industry today and are considered to be recalcitrant, non-biodegradable and persistent (Stolz, 2001; Gupta and Suhas, 2009; Salleh et al., 2011).

1.3.1 Azo Dyes

Today, nearly one million tons of dyes are produced annually in the world of which azo dyes represent about 70% by weight. The chromophoric system consists essentially of one or more azo groups, (-N=N-), in association with one or more aromatic systems as shown in Fig. 1.1.

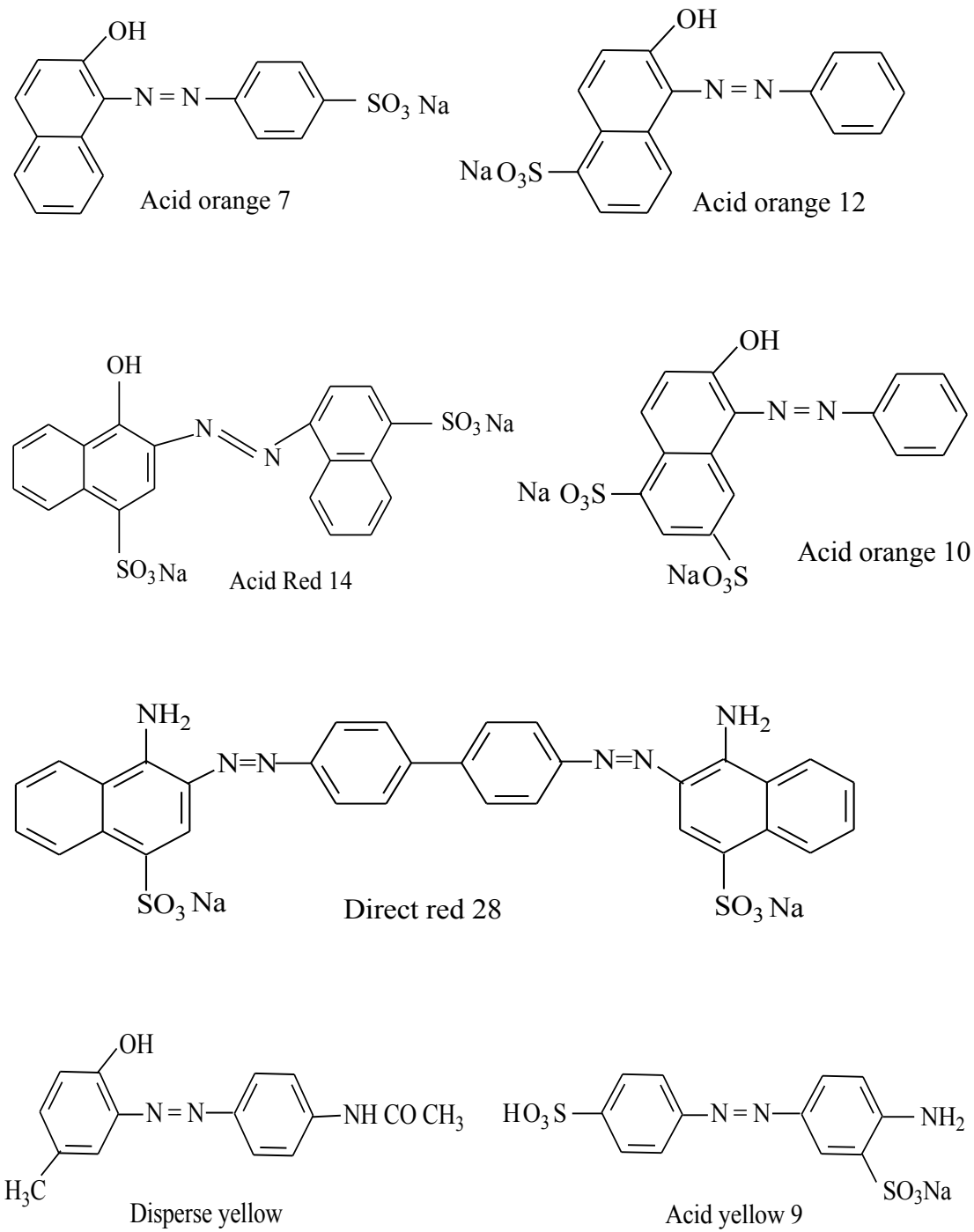


Fig. 1.1: Chemical structures of different types of azo dyes.

Sulfonated azo dyes are the most numerous of the manufactured synthetic azo dyes in which the sulfonic acid groups are introduced to increase the water solubility of the dye and the azo group confer resistance to microbial attack (Vijaykumar et al., 2007). These azo dyes are widely used in a number of industries such as textile, food, cosmetics, pharmaceuticals, plastics, paper printing and pulp, leather and so on. Approximately, 10-15% of azo dyes are released into the environment during manufacturing and usage which have myriads of structural varieties (Stolz, 2001; Rai et al., 2005). Most of the azo dyes are generally stable under exposure to light and washing, and also recalcitrant to biodegradation in conventional activated sludge treatment due to their xenobiotic toxicity (Puvaneswari et al., 2006; Pandey et al., 2007; Liu et al., 2009). Typically, soluble colored compounds are responsible for 24 to 35% of the waste COD and 90 to 95% of the waste color (total absorbance); the suspended and colloidal colored compounds account for the remaining small fraction of the color (Hao et al., 2000).

The electron withdrawing characteristics of the azo group and specific substitution patterns generate an electron deficiency, and thus make azo dyes resistant to oxidative catabolism. However, azo dyes are electron-deficient xenobiotic compounds and they are capable to be reductively degraded via azo reduction in anaerobic conditions, yielding aromatic amines intermediates (Stolz, 2001; Pandey et al., 2007). The latter compounds, in turn, generally require aerobic conditions for their degradation. Therefore, without adequate treatment, these azo dyes and their intermediates can remain in the environment for an extended period of time causing

numerous environmental problems. It has been reported that the half-life of hydrolyzed Reactive Blue 19 (RB19) is about 46 years at pH 7 and 25 °C (Hao et al., 2000).

1.4 Environmental Concerns

Public perception of water quality is greatly influenced by the color which is the first contaminant to be recognized in wastewater. The presence of color and its causative compounds have always been undesirable in water used for either industrial or domestic needs (Rai et al., 2005; Crini, 2006). Apart from the aesthetic problems, the greatest environmental concern with the dyes is their absorption and reflection of sunlight entering the water. This interferes with the growth of bacteria and plants, causing a disturbance of the ecology of receiving waters. Thus, the discharge of dyes to the environment has become an environmental hazard to human health as well as aquatic lives. This is because of the low biodegradability and the toxic nature of the dyes.

Azo dyes have become a major concern in wastewater treatment because many of them are recalcitrant, resistant to the natural aerobic digestion, and are stable to light, heat, and oxidizing agents (Brown and de Vito, 1993; Sponza and Işık, 2005; Işık and Sponza, 2007). Further, many azo dyes are made from known carcinogens, such as benzidine, naphthalene and other aromatic compounds which might be transformed as a result of microbial metabolism (Crini, 2006; Chen et al., 2009). Numerous reports indicate that textile azo dyes and effluents have toxic effects on the germination rates and biomass of several plant species which have important ecological functions, such as providing a habitat for wildlife, protecting soil from erosion and providing the organic

matter that is so significant to soil fertility (Ghodake et al., 2008; Saratale et al., 2011). Furthermore, it has been reported that azo and nitro compounds are reduced in sediments and in the intestinal environment, resulting in the generation of the parent toxic amines (Chung et al., 1992; Pinheiro et al., 2004). Anthraquinone-based dyes are the most resistant for degradation due to their fused aromatic structure and thus remain colored for long periods of time (Çınar et al., 2008). Benzidine-based azo dyes have been found to be tumorigenic and carcinogenic due to their biotransformation to benzidine (Pinheiro et al., 2004; Vijaykumar et al., 2007).

As a result of this, legislation controlling the use of such substances is being developed in various countries (Rai et al., 2005). As laws became more stringent, the textile industry around the world has begun using innovative methods for wastewater remediation, more so for the water containing the residual color from the dyes that remains almost unaffected by the conventional aerobic treatment systems. In light of these facts, attention has now been focused on the efficient removal of dyes from the environment. However, as compared to the growth of the dye industries and dye products, relatively little progress has been made towards their removal (Rai et al., 2005).

1.5 Dye Removal Techniques

Current trends dictate that the development of dye removal techniques needs to be safer, greener and cleaner. To date, several physico-chemical and biological methods have been developed to treat dye-containing wastewaters including membrane filtration, coagulation/flocculation, precipitation, flotation, adsorption on inorganic or organic

matrices, ion exchange, ion pair extraction, ultrasonic mineralization, electrolysis, advanced oxidation (chlorination, bleaching, ozonation, Fenton oxidation and photo-catalytic oxidation) and chemical reduction. Biological pre-treatment, main treatment and post treatment techniques include bacterial and fungal (microbiological or enzymatic decomposition), bio-sorption and biodegradation in aerobic, anaerobic, anoxic or combined anaerobic/aerobic treatment processes can be employed to remove color from dye containing wastewaters as reviewed by researchers (Robinson et al., 2001; Forgacs et al., 2004; Gupta and Suhas, 2009). Combination of different techniques involving primary or tertiary treatment such as ozonation, Fenton's reagent, electrochemical destruction and photo-catalysis has been applied in the removal of azo dye-containing wastewater. However, such technologies usually involve complicated procedures and are costly (Pearce et al., 2003).

Adsorption is one of the most widely used techniques to remove azo dyes due to its effectiveness and economical advantages (Hao et al., 2000; Gupta and Suhas, 2009). However, the main disadvantage of such a technique is the progressive loss of adsorptive capacity of the adsorbent with use. Currently, microbial degradation has become a promising approach for dye treatment because it is cheaper, effective and more environmentally friendly. The ability of microorganisms to carry out dye decolorization has received much attention. In this context, a hybrid treatment of azo dye involving adsorption technique followed by microbial treatment to regenerate the azo dye-loaded adsorbent under sequential or simultaneous approach is a good alternative method to remove azo dye (Walker and Weatherley, 1998; Aktas and Çeçen, 2007; Ip et al., 2010).

1.5.1 Adsorption

Adsorption is defined as a process wherein a material is concentrated at a solid surface from its liquid or gaseous surroundings *via* two types of attractions; namely physical and/or chemical interactions (Gupta and Suhas, 2009). Generally, if the attractive forces between the adsorbed molecules and the solid surface are van der Waals forces, the process is called physical adsorption and these forces are weak in nature resulting in reversible adsorption. On the other hand, if adsorption occurred when chemical bonds are formed between the molecules and the solid surface, it is difficult to remove chemisorbed species from the solid surface in view of the higher strength of the bonding (Gupta and Suhas, 2009).

The adsorption technique is considered to be one of the most effective and proven physico-chemical techniques having potential applications in both water and wastewater treatment. Therefore, adsorption has wide applicability in dye-containing wastewater using a wide range of adsorbents as reported in the literature (Bousher et al., 1997; Robinson et al., 2001; Forgacs et al., 2004). The adsorption of synthetic azo dyes on inexpensive and efficient solid adsorbents is considered as a simple and economical method for their removal from water and wastewater. The adsorption characteristics of a wide variety of inorganic and organic adsorbents have been determined and their capacity to remove synthetic azo dyes has been evaluated (Armagan et al., 2004; Al-Degs et al., 2007; Donia et al., 2009; Cotoruelo et al., 2010; Errais et al., 2011; Li et al., 2011; Parker et al., 2012).

1.5.1.1 Activated Carbon as Adsorbent

The history of carbon adsorption in the purification of drinking water and wastewater dates back to ancient times followed by observations made by Lowitz in 1785 of the reversible removal of color and odor from water by wood charcoal (Gupta and Suhas, 2009). In addition, activated carbon adsorption has been cited by the US Environmental Protection Agency as one of the best available environmental control technologies (Moreno-Castilla, 2004). Activated carbons present an outstanding adsorption capacity that stems from their surface area, pore structure and surface chemical properties. Activated carbons usually outperformed most adsorbents in removing dyes from solution with high adsorption capacities for anionic and cationic dyes (Gupta and Suhas, 2009). In order to demonstrate the versatility of activated carbon, different researchers have used this adsorbent for the removal of different types of dyes (Walker and Weatherley, 1998, 1999; Özacar and Şengil, 2002; Faria et al., 2004; Al-Degs et al., 2008; El Qada et al., 2008; Valderrama et al., 2008; Lu et al., 2011).

Faria et al. (2004) evaluated the influence of surface chemical groups of an activated carbon (AC) on the removal of different classes of dyes. Their results have shown that the surface chemistry of the AC plays a key role in dye adsorption performance and the basic sample obtained by thermal treatment under H₂ flow at 700 °C was the best material for the adsorption of all the investigated dyes, namely an acid, a basic and a reactive dyes with the maximum dye adsorption capacities of 310 mg/g, 190 mg/g, and 546 mg/g, respectively.

Valderrama et al. (2008) described the adsorption of an azo dye of Acid Red 14 from aqueous solutions onto granular activated carbon (GAC) in a batch system. They found that the maximum dye adsorption capacity of GAC was 31 g/kg at neutral and basic pH values.

An investigation into the adsorption behavior of reactive dyes on activated carbon was carried out under various experimental conditions of pH, ionic strength, and temperature (Al-Degs et al., 2008). The results show the relatively high adsorption capacities of activated carbon for reactive dyes; namely Reactive Blue 2, Reactive Yellow 2, and Reactive Red 4 of 0.27 mmol/g, 0.24 mmol/g, and 0.11 mmol/g, respectively, due to the large surface area of AC adsorbent (820 m²/g) and a modest surface charge density (0.54 group/nm²).

Al-Qada et al. (2008) compared the adsorption capacities of different basic dyes of Methylene Blue (MB), Basic Red (BR) and Basic Yellow (BY) onto different types of activated carbons produced by steam activation, respectively, in small laboratory scale and large industrial scale processes under batch system. It was found that the activated carbon produced from New Zealand coal using steam activation has the highest adsorptive capacity towards MB dye of 588 mg/g.

All these studies have shown that activated carbons are good materials for the removal of different dyes in general. However, high procuring, processing cost and non-selectivity restrict activated carbon's use in many countries besides the regeneration difficulties of the spent activated carbon. On prolonged contact with dyes, the available adsorption sites become exhausted with adsorbed dye and eventually the AC loses its adsorptive capacity. The increased utilization of AC in recent years has resulted in the

development and broader application of a number of new regeneration processes which increase the service period of AC. However, any regeneration process results in a loss in adsorption capacity in comparison with the fresh AC (Robinson et al., 2001; Gupta and Suhas, 2009; Nath and Bhakhar, 2011). For instance, thermal regeneration of the spent AC normally results in 5-10% loss of the AC due to oxidation and attrition. This has promoted search by various investigators for alternative cost effective adsorbents which may replace activated carbons in pollution control through adsorption processes.

Different types of low cost adsorbents have been used for the removal of azo dyes such as fly ash (Chatterjee et al., 2010), hazelnut shell and sawdust (Ferrero, 2007), soy meal hull (Arami et al., 2006), rice husk (Mohamed, 2004), microalgae (Cardoso et al., 2012), animal bone meal (El Haddad et al., 2012), banana peel (Amela et al., 2012), modified sugarcane bagasse (Gusmão et al., 2013), etc. However, the drawbacks of these natural adsorbents are long contact time and also low adsorption capacity. Besides, accumulation of these cheap spent adsorbents creates a disposal problem. Chitin and chitosan which are polysaccharides with chemical structures similar to cellulose were found to be good adsorbents to remove azo dyes (Chatterjee et al., 2007; Wan Ngah et al., 2011; Peng et al., 2013) although these biopolymers are susceptible to microbial attack.

Recently, inorganic adsorbents have gained special attention in the removal of dyes from the aqueous solutions due to their resistance to the shrinking/swelling, good mechanical, thermal and chemical stability and resistance to microbiological degradation (Forgacs et al., 2004). Different inorganic adsorbents have been used to remove acid dyes such as bentonite (Bouberka et al., 2005; Gök et al., 2010), clay

(Errais et al., 2012; Arellano-Cárdenas et al., 2013), calcined alunite (Özacar and Şengil, 2002), peat (Allen et al., 2004), Kaolinite (Khan et al., 2012), montmorillonite (Bouberka et al., 2006), titania–silica composite (Messina and Schulz, 2006), activated bauxite and fullers earth (Lambert et al., 1997) and silica gel (Alexander et al., 1978; Karim et al., 2012). Nowadays, silica gel and its surface modification have gained great research interest for the removal of dye, specifically azo dyes (Anbia and Salehi, 2012; de Menezes et al., 2012; Hak-Sung et al., 2012; Liu et al., 2013) due to the high possibility of tailoring its physical and/or chemical properties to optimize its selectivity and performance.

1.5.1.2 Modified Silica Gel as Adsorbent

Modification of the surface of silica gel with different chelating agents as an organic-inorganic hybrid adsorbent for the removal of azo dyes from aqueous solutions has received great attention nowadays due to its fast kinetic adsorption, controlled porosity and chemical reactivity of its surface, very low degree of swelling/shrinking, resistance to the microbial attack, high selectivity and good adsorption capacity (Phan et al., 2000; Ho et al., 2003; Yoshida et al., 2003; Jal et al., 2004; Jesionowski, 2005; Parida et al., 2006; Kannan et al., 2008; Pavan et al., 2008; Donia et al., 2009; Samiey and Toosi, 2010; Huang et al., 2011). What makes silica gel attractive for dye wastewater treatment is the possibility of tailoring their physical and/or chemical properties in order to optimize their performance (Impens et al., 1999; Ho et al., 2003; Jal et al., 2004). Many researchers have functionalized silica gel surface to remove azo dyes from aqueous solutions (Asouhidou et al., 2009; Atia et al., 2009; ar al et al.,

2010; de Menezes et al., 2012; Karim et al., 2012). Silica gel functionalized with monochloro-triazinyl β -cyclodextrin was used for the removal of Acid Blue 25 and the adsorption capacity was found to be 45.80 mg/g (Phan et al., 2000).

Ho et al. (2003) prepared modified ordered mesoporous silica (OMS) adsorbents by grafting amino- and carboxylic-containing functional groups onto MCM-14 for the removal of Acid Blue 25 and Methylene Blue dyes from wastewater. They found that the amino-containing OMS-NH₂ adsorbent has a large adsorption capacity and a strong affinity for the Acid Blue 25 whereas the OMS-COOH is a good adsorbent for Methylene Blue displaying an excellent adsorption capacity and selectivity for the dye. Furthermore, these adsorbents can be regenerated by simple washing with alkaline or acid solution to recover both the adsorbent and the adsorbate (dye).

The removal of Basic Blue 9 and Acid Orange 52 dyes using modified silica with *N*-2-(aminoethyl)-3-aminopropyltriethoxysilane has been investigated by Jesionowski (2005). The adsorption capacities were found to be 1.2 and 0.261 $\mu\text{mol}/\text{m}^2$ for Basic Blue 9 and Acid Orange 52, respectively.

Pavan et al. (2008) synthesized the hybrid anilinepropylsilica xerogel (SiAn) and used it as an adsorbent for removing Congo Red from aqueous solutions using batch system. The dye adsorption equilibrium was rapidly attained after 20 min of contact time with the maximum adsorption capacity of 22.62 mg/g of Congo Red .

The meso-structured silica nanoparticles (MSN_{AP}) were synthesized by modification with 3-aminopropyl triethoxysilane (APTES) and their performance was tested by the adsorption of Methylene Blue (MB) dye in batch system under different conditions such as pH, adsorbent dosage, initial MB concentration (Karim et al.,

2012). The results revealed that the best conditions were achieved at pH 7, 0.1 g/L adsorbent dosage, and an initial MB concentration of 60 mg/L.

Development of an ionic silica-based hybrid material containing the cationic pyridinium group (Py) was carried out and the modified silica particles, namely Py/Si-90, Py/Si-92 and Py/Si-94, respectively, were employed for the removal of the Reactive Red 194 textile dye from aqueous solution (de Menezes et al., 2012). The dye-removing ability of these adsorbents was determined by the batch contact adsorption procedure. The maximum adsorption capacities were 165.4, 190.3 and 195.9 mg/g for Py/Si-90, Py/Si-92 and Py/Si-94, respectively. The dye-loaded adsorbents were regenerated by using 0.4 M NaOH solution as an eluent with an efficiency of 98.2%.

Monoamine-modified silica particles (MAMS) had been synthesized by Donia et al. (2009) using 3-aminopropyltriethoxysilane (3-APTS) and used to remove Acid Orange 10 (AO10) and Acid Orange 12 (AO12) from their aqueous solutions. The adsorption capacities were 35.50 and 14.29 mg/g for AO10 and AO12, respectively. The loaded MAMS with the investigated azo dyes can be regenerated by washing with alkaline solution of NaOH at pH 10 to recover the adsorbent (MAMS) and adsorbate (azo dye).

Atia et al. (2009) have synthesized two silica samples through precipitation of commercial silica in the presence and absence of magnetite particles (Fe_2O_3). The two silica samples were immobilized with 3-aminopropyltriethoxysilane to give monoamine precipitated modified silica (MAMPS) and mono-amine modified magnetic silica (MAMMS). The two silica samples were used to remove Acid Orange 10 (AO10) from its aqueous solutions under different operational conditions, namely contact time, pH,

and different initial concentrations of the azo dye. The maximum adsorption capacities of AO10 onto MAMPS and MAMMS were found to be 48.98 and 61.33 mg/g, respectively. The AO10-loaded MAMPS and MAMMS were chemically regenerated using NaOH (pH 10) with an efficiency of 98% over three adsorption/desorption cycles.

All these studies have demonstrated that there are many different types of modified silicas which could be used in the removal of dyes from aqueous solutions in relatively short contact time, specifically for azo dyes. Among these different types of modified silicas, mono-amine modified silica (MAMS) was found to be a good adsorbent for azo dye removal due to the greener protocol used for its synthesis as described by Donia et al. (2009). Donia et al. (2009) synthesized MAMS particles using distilled water and under the room temperature of 26 °C instead of using the common organic solvent such as toluene and the heating requirements at *ca.* 85 °C as reported in the literature (Zhao et al., 2012; Ghosh et al., 2013). Further, it has relatively high adsorption capacity and high possibility to be regenerated. Therefore, MAMS adsorbent was chosen in this study to remove different types of mono azo dyes, namely AO7, AY9 and AR14 and the spent MAMS to be regenerated biologically.

1.5.2 Biodegradation of Azo Dyes

The literature shows that various microorganisms such as fungi (Hadibarata et al., 2012), bacteria (Tony et al., 2009), yeast (Martorell et al., 2012), and algae (El-Sheekh et al., 2009) possess the potential to decolorize or even mineralize azo dyes. In fact, bacterium is the most widely studied microorganism and is used in azo dye decolorization/mineralization due to its widespread high growth rate and adaptability.

Azo dyes can be completely decomposed by a series of bacterial reactions (biological assimilation) initiated by azoreductase-catalyzed reduction to cleave the azo bonds under anaerobic conditions to relatively simple intermediate amine products as presented in Fig. 1.2. The produced aromatic amines might be toxic and resist further anaerobic degradation (Puvaneswari et al., 2006; Chen et al., 2009; Solís et al., 2012).

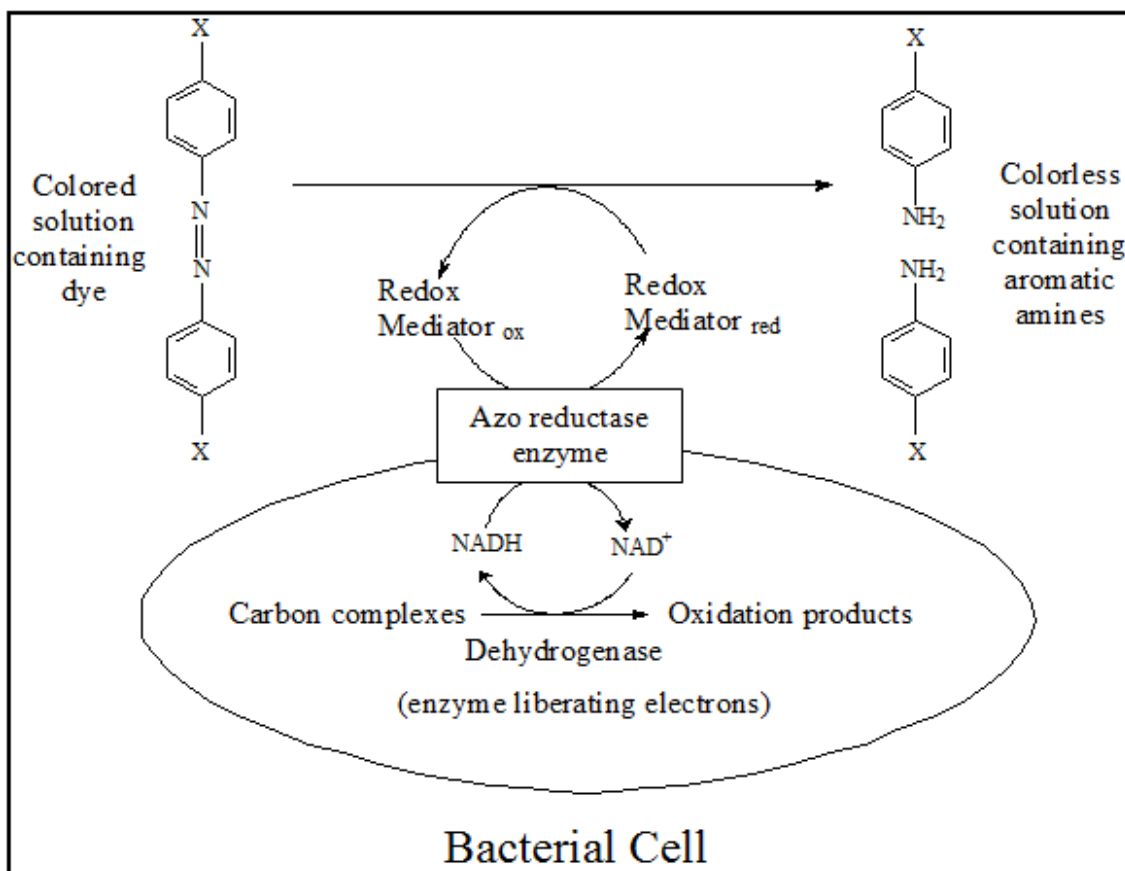


Fig. 1.2: Proposed mechanism for reduction of azo dye by whole bacterial cells (Keck et al., 1997; Stolz, 2001).

The application of aerobic conditions could completely mineralize some biodegradable aromatic amines as reported in the literature (Pearce et al., 2003; Saratale et al., 2011; Solís et al., 2012). Therefore, combined anaerobic/aerobic systems are necessary for complete azo dye biodegradation as reviewed by van der Zee and Villaverde (2005).

The fate of azo dyes and aromatic amines using anaerobic-aerobic treatment is shown in Fig. 1.3.

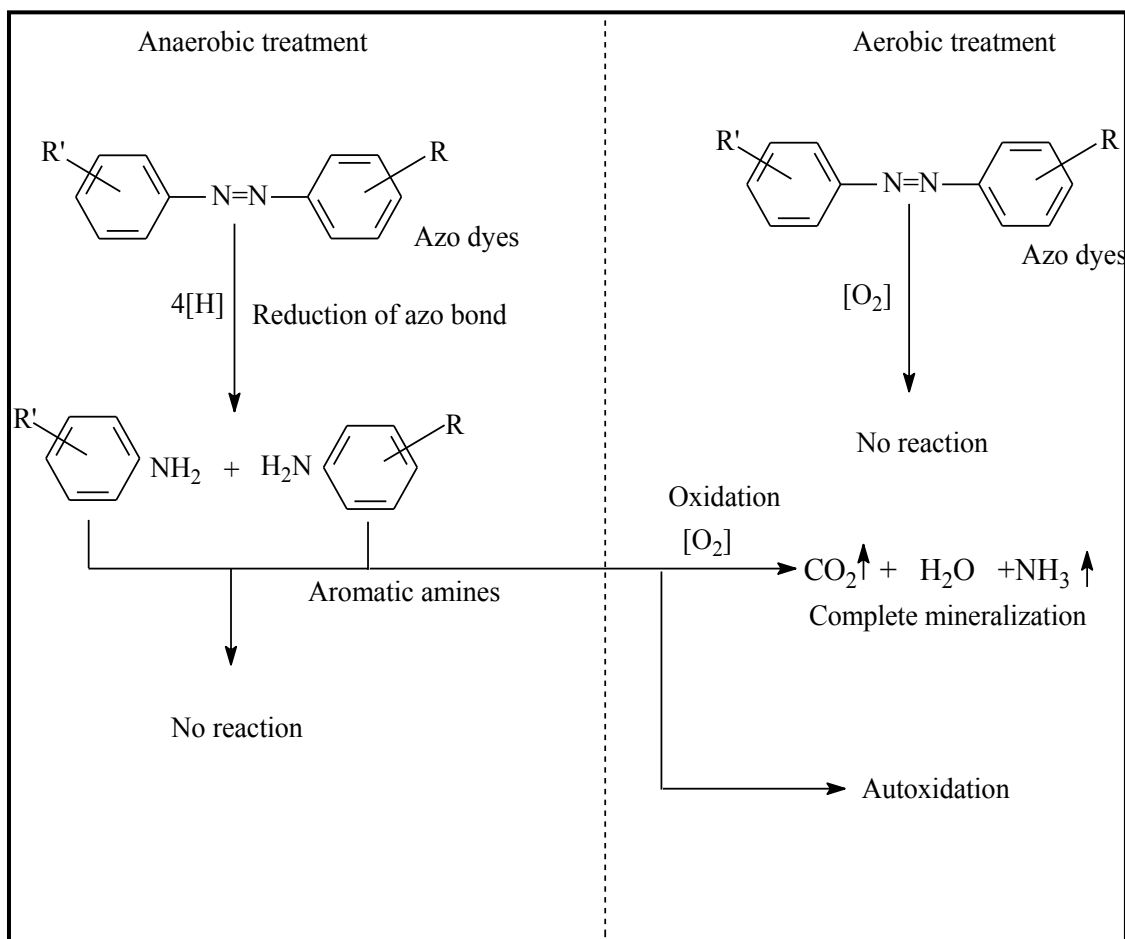


Fig. 1.3: General overview of the fate of azo dyes and aromatic amines during anaerobic-aerobic treatment (van der Zee and Villaverde, 2005).

The aromatic amines compounds could be bio-mineralized under aerobic conditions by non-specific enzymes through hydroxylation and ring-fission of aromatic compounds (Ong et al., 2005; Carvalho et al., 2008), though not all aromatic amines can be completely mineralized (van der Zee and Villaverde, 2005). In contrast to the reports of anaerobic bio-decolorization of azo dyes, other studies have reported that some azo dyes could be aerobically bio-decolorized (Coughlin et al., 2002; Buitrón et al., 2004; Venkata Mohan et al., 2007; Tony et al., 2009; Khouni et al., 2012; Venkata Mohan et al., 2012).

Further, a recent study reported that Acid Red 88 (AR88) could be decolorized in anoxic up-flow fixed-film column reactor and the effluent of an anoxic column reactor was fed to a continuously stirred aerobic reactor to mineralize the produced AR88 intermediates (Khehra et al., 2006). However, the main interest in anaerobic conditions has been focused on bacteria from the human intestine that are involved in the metabolism of azo dyes ingested as food additives (Stolz, 2001).

Farabegoli et al. (2010) studied the decolorization of mono-azo dye of Reactive Red 195 (RR195) by a mixed culture in a laboratory scale alternating anaerobic-aerobic sequencing batch reactor (SBR) in the presence of biodegradable carbon source under different operational conditions of sludge retention time (SRT), hydraulic retention time (HRT), influent color and organic carbon loading. They found that the optimal operating conditions for maximum color efficiency of 97% were 40 mg/L of RR195, 800 mg/L influent of COD, 50 d SRT, and a 24 h-cycle. Some inhibition was present at influent color loadings above 40 mg/L.

Hakimelahi et al. (2012) investigated the biological treatment of wastewater containing an azo dye of Acid Red 18 using mixed culture in alternating anaerobic/aerobic SBRs using different azo dye concentrations in the range of 0-230 mg/L. The study showed that the majority of the dye removal was observed in the anaerobic stage whereas the aerobic contributions were insignificant in color removal. The average COD removal of no lower than 85% was achieved while the remaining COD originated from Acid Red 18 and its degradation products.

Khouni et al. (2012) studied the treatment of reconstituted textile wastewater containing a widely used textile reactive dye in an aerobic SBR using a novel bacterial consortium under different volumetric dye loading rates (3-20 g dye/m³.d) at room temperature and pH 7. The study showed that the acclimated novel microbial consortia “Bx” displayed the highest purification capabilities under aerobic conditions giving maximum decolorization rates in the range of 88-97% and COD removal percentages of about 95-98% when the volumetric dye loading rates were increased to 15 g dye/m³ d. The mean rates of decolorization and COD removal decreased to 70% and 90%, respectively when the volumetric dye loading rate was increased to 20 g dye/m³.d.

Mohan et al. (2012) evaluated the functional behavior of anoxic-aerobic-anoxic microenvironment on the azo dye of Acid Black 10B in a periodic discontinuous batch mode operation for 26 cycles. They found that the dye removal efficiencies and azo-reductase activity increased with each feeding event until the 13th cycle indicating the stable proton shuttling between metabolic intermediates providing higher number of reducing equivalents towards dye degradation. The integration of anoxic

microenvironment with aerobic operation might have facilitated effective dye mineralization due to the possibility of combining redox functions.

The above observations indicate that the anaerobic and/or aerobic systems are effective in the bio-decolorization/bio-mineralization of azo dyes. However these systems require complicated designs to suit the stringent conditions used such as N₂ supply and/or O₂ aeration continuously in closed systems. Therefore, studies on bio-decolorization/bio-mineralization of azo dye under anoxic/aerobic conditions using single bio-reactor SBR in opened system are required due to: (i) simplicity in design, (ii) cost saving as it is more economical to operate compared to fully aerobic and/or anaerobic operated SBRs due to less aeration requirements using oxygen (aerobic-SBR) or nitrogen (anaerobic-SBR), (iii) less accumulation of toxic bio-degradable intermediates compared to anaerobic operated SBR, and (iv) ability to be operated in open system. To date, no study has been reported on the bio-decolorization of azo dyes, COD removal and the performance of the mixed bacterial culture using sequential anoxic-aerobic REACT operated SBR as a single bioreactor.

1.6 Regeneration of Spent Adsorbent

Activated carbon (AC) and other adsorbents were widely used in removing the dyes as described in Section 1.5.1.1. After adsorption, the AC and other adsorbents saturated with dyes become a secondary waste and will need to be discarded, incinerated or regenerated. Disposal of the loaded adsorbent is not acceptable due to (i) the potential of re-contamination of the environment with the azo dye and (ii) the high cost of some commercial adsorbents such as granular activated carbon. Incineration of

the spent adsorbent is also not a good option due to (i) produced greenhouse gases and (ii) the possibility of destroying the adsorbent structure or the organic chelating groups on the modified adsorbent. In this context, regeneration seems to be a proper method to clean up the spent adsorbent surface. The importance of the regeneration process has stimulated intense research in this field. A variety of regeneration attempts have been proposed by many researchers to regenerate the spent adsorbent and increase its service life, especially carbon saturated with organic pollutants, such as phenol and its derivatives (Chiang et al., 1997; Laszlo, 2000; Shende and Mahajani, 2002; Sabio et al., 2004; Purkait et al., 2007; Weng and Hsu, 2008; Qu et al., 2009; Oh et al., 2011; Ren et al., 2013; Toh et al., 2013). There are several well-established methods for the regeneration of spent adsorbent that can be classified in three abroad groups: physical, chemical, and biological regeneration methods. However, methods in current use are either not efficient enough or too expensive.

1.6.1 Physical Regeneration

Physical regeneration has been used to regenerate the spent adsorbent, especially for spent activated carbon, under different techniques such as thermal regeneration (Moreno-Castilla et al., 1995; Chiang et al., 1997; Sabio et al., 2004; Wang et al., 2006; Wei et al., 2013), wet oxidation regeneration (Mvndale et al., 1991; González et al., 2002; Shende and Mahajani, 2002; Okawa et al., 2007), ultrasonic regeneration (Hamdaoui et al., 2003; Juang et al., 2006), dielectric barrier discharge plasma regeneration (Qu et al., 2009; Lu et al., 2012), microwave irradiation regeneration (Polaert et al., 2010; Wang et al., 2010; Foo and Hameed, 2012), solar regeneration

(Yap and Lim, 2012) and electrochemical regeneration (Zhang, 2002; Brown et al., 2004; Garcia-oton et al., 2005; Narbaitz and Karimi-Jashni, 2008; Weng and Hsu, 2008; Berenguer et al., 2010; Mohammed et al., 2011; Conti-Ramsden et al., 2012; Hussain et al., 2013).

Thermal volatilization usually refers to the process of drying, thermal desorption and high temperature heat treatment in the presence of limited amount of oxidizing gases such as water vapor, flue gas and oxygen (Nath and Bhakhar, 2011). Thermal regeneration is widely used due to its simplicity and high efficiency. However, it has some important disadvantages such as (1) high cost in terms of installation and energy consumption to keep the regeneration temperature at about 800 – 850 °C, (2) time consuming and (3) carbon loss of 10-20% by weight due to attrition, burn-off and washout (Berenguer et al., 2010), (4) the necessity of *ex situ* operation, that is, the transportation of the exhausted carbon to a reactivation center for regeneration and transported back to the in-process plant (Berenguer et al., 2010) and (5) the release of substantial amounts of CO₂ into the environment as well (Chiang et al., 1997; Álvarez et al., 2004). Further, adsorbates from adsorbents are released into the atmosphere in reactive, oxidized and partially oxidized states (Nath and Bhakhar, 2011).

Thermal regeneration has been used to regenerate two different types of zeolite (natural and synthetic zeolite MCM-22) loaded with basic dye of Methylene Blue (Wang et al., 2006). Regeneration of Methylene Blue-loaded MCM-22 (synthetic zeolite) by high temperature treatment can make the adsorbent exhibit comparable or superior adsorption capacity as compared to the fresh sample depending on the